Title:

A novel irreversible TEAD inhibitor, SWTX-143, blocks Hippo pathway transcriptional output and causes tumor regression in preclinical mesothelioma models

Authors:

Hanne Hillen[1*], Aurélie Candi[2*], Bart Vanderhoydonck[2], Weronika Kowalczyk[1], Leticia Sansores-Garcia[1], Elena C. Kesikiadou[1], Leen Van Huffel[1], Lore Spiessens[1], Marnik Nijs[2], Erik Soons[2], Wanda Haeck[2], Hugo Klaassen[2], Wim Smets[2], Stéphane A. Spieser[2], Arnaud Marchand[2], Patrick Chaltin[2], Fabrice Ciesielski[4], Francois Debaene[4], Lei Chen[3], Adeela Kamal[3], Stephen L. Gwaltney[3], Matthias Versele[2] and Georg A. Halder[1#]

Affiliations:

[1] VIB Center for Cancer Biology and KU Leuven Department of Oncology, KU Leuven, Leuven, Belgium

[2] Center for Drug Design and Discovery (CD3), KU Leuven, Leuven, Belgium – Cistim Leuven vzw, Leuven, Belgium

[3] SpringWorks Therapeutics, Stamford, Connecticut, USA

[4] NovAliX, Campus Guy Ourisson, 16 rue d'Ankara, 67080 Strasbourg, France

[*] Equal contribution

[#] Corresponding author

Running title: A novel TEAD inhibitor

Key words: Mesothelioma, Hippo, YAP, inhibitor, cancer therapy

Financial Support: This work was supported by SpringWorks Therapeutics internal funding and a Stichting Tegen Kanker grant (ZKE0232-02-W01)

Corresponding author: Georg Halder, VIB Center for Cancer Biology and KU Leuven Department of Oncology, KU Leuven, Leuven, Belgium. Email: georg.halder@kuleuven.be

Conflicts of interest: H.H., A.C., B.V., W.K., L.S., E.K., L.VH., L.S., M.N., E.S., W.H., H.K., W.S., S.S., A.M., P.C., L.C., A.K., L.G., M.V., G.H. have established a license and collaboration agreement with SpringWorks therapeutics around the submitted work. VIB, CD3 (KU Leuven) and SpringWorks therapeutics have applied for a patent (WO/2022/072741) around the submitted work. F.C. and F.D. declare no conflict of interest.

Word count: 5400**, Number of figures**: 5 + 4 supplemental

ABSTRACT

The Hippo pathway and its downstream effectors, the YAP and TAZ transcriptional co-activators, are deregulated in multiple different types of human cancer and are required for cancer cell phenotypes *in vitro* and *in vivo*, while largely dispensable for tissue homeostasis in adult mice. YAP/TAZ and their main partner transcription factors, the TEAD1-4 factors, are therefore promising anti-cancer targets. Due to frequent YAP/TAZ hyperactivation caused by mutations in the Hippo pathway components *NF2* and *LATS2*, mesothelioma is one of the prime cancer types predicted to be responsive to YAP/TAZ-TEAD inhibitor treatment. Mesothelioma is a devastating disease for which currently no effective treatment options exist. Here, we describe a novel covalent YAP/TAZ-TEAD inhibitor, SWTX-143, that binds to the palmitoylation pocket of all four TEAD isoforms. SWTX-143 caused irreversible and specific inhibition of the transcriptional activity of YAP/TAZ-TEAD in Hippo-mutant tumor cell lines. More importantly, YAP/TAZ-TEAD inhibitor treatment caused strong mesothelioma regression in subcutaneous xenograft models with human cells and in an orthotopic mesothelioma mouse model. Finally, SWTX-143 also selectively impaired the growth of *NF2*-mutant kidney cancer cell lines, suggesting that the sensitivity of mesothelioma models to these YAP/TAZ-TEAD inhibitors can be extended to other tumor types with aberrations in Hippo signaling. In brief, we describe a novel and specific YAP/TAZ-TEAD inhibitor that has potential to treat multiple Hippo-mutant solid tumor types.

INTRODUCTION

The Hippo pathway has emerged as a promising target for cancer therapy due to the prominent hyperactivation of the Hippo pathway effectors YAP and TAZ in many human solid cancer types [1–6]. YAP and TAZ are transcriptional co-activators that form a complex with partner transcription factors, primarily with the TEAD transcription factors [1–6]. The TEAD transcription factors have 4 paralogs, TEAD1-4, that share highly conserved DNA binding and YAP/TAZ interaction domains. The binding of YAP and TAZ to TEADs stimulates the expression of target genes such as *CYR61, CTGF*, *CCND1* and *MYC* that promote cell proliferation, survival and plasticity [1–6]. In normal homeostasis, the Hippo pathway core kinases LATS1/2 phosphorylate and regulate the stability and nuclear localization of YAP and TAZ thereby preventing their inductive

effect on target gene expression. Indeed, YAP/TAZ are largely dispensable for normal homeostasis of adult mice, showing no overt phenotypes upon genetic co-deletion of *Yap* and *Taz* in many different adult organs [2,5,7–9]. However, when YAP/TAZ are hyperactivated, for example by loss-of-function mutations in *LATS1/2*, unphosphorylated YAP/TAZ can translocate to nucleus and activate transcription of downstream target genes thereby driving tumor progression, metastasis and therapy resistance [10,11]. Thus, the broad activation of YAP/TAZ in solid tumors, their importance for cancer cell phenotypes but their irrelevance for homeostasis makes them promising targets for cancer therapy.

Mesothelioma is the primary indication for treatment with YAP/TAZ-TEAD inhibitors due to the high frequency of mutations in Hippo pathway components [12–15]. Mesothelioma is a highly aggressive cancer that originates from the mesothelium, an epithelial cell layer that covers the lungs (pleura), heart (pericardium) and abdominal cavity (peritoneum) and that provides a non-adhesive surface to allow organ movement [16]. However, most mesothelioma develop in the pleura and are called malignant pleural mesothelioma (MPM). Around 80% of all MPM cases are linked to asbestos exposure and the disease is often diagnosed at advanced stages after a long latency resulting in a poor prognosis [16]. Currently, no effective therapies are available [17]. Genetic and transcriptional analyses showed that mutations in genes encoding Hippo pathway components are very frequent (up to 75%) with *NF2* or *LATS2* being affected in up to 50% of malignant pleural mesotheliomas [13–15]. Also, knockdown of *YAP* in mesothelioma cells impaired cell growth, invasion and tumor formation [12,18]. Therefore, targeting the Hippo pathway is predicted to be an effective treatment for at least a subgroup of mesothelioma.

Several compounds have been identified that inhibit the effects of YAP/TAZ [19–23]. Based on their mechanism of action, they can be classified into (I) compounds that stimulate the upstream kinases of the Hippo pathway thereby causing the inhibition of YAP/TAZ activity, (II) compounds that target YAP/TAZ or TEAD directly and interfere with their binding, and (III) compounds that act on target genes downstream of YAP/TAZ-TEAD [19,24]. Recent reports describe a novel class of small molecule YAP/TAZ-TEAD inhibitors including K-975 [20] and VT104 [21], that bind (covalently or non-covalently) into a hydrophobic palmitoylation pocket (so-called P-pocket) of the

TEADs, where they interact with a cysteine residue located at the entrance of the P-pocket [25,26]. Palmitoylation of TEAD proteins is essential for their stability and activity, and compound binding blocked auto-palmitoylation and YAP/TAZ binding [25,27–30]. These P-pocket inhibitors thus blocked expression of canonical Hippo pathway target genes such as *CYR61, CTGF, IGFBP3* and *NPPB* in different mesothelioma model systems and suppressed the growth of xenograft tumors from Hippo-mutant mesothelioma cell lines [19–23]. These results show that P-pocket binders inhibit YAP/TAZ-TEAD transcriptional activity and suppress mesothelioma tumor growth in vitro and in vivo.

While mutations in Hippo pathway genes are common in malignant pleural mesothelioma, genetic hyperactivation of YAP/TAZ-TEAD occurs in a variety of other solid tumor types [1–6,31]. In particular, biallelic inactivation of *NF2* commonly occurs in aggressive kidney cancer subtypes including clear cell renal cell carcinoma (ccRCC) with sarcomatoid dedifferentiation (19%) [32,33], type II papillary RCC (pRCC; 13%) [34–36] and unclassified RCC (uRCC; 18%) [37], for which there are no good therapies. Using inducible knockout of *Yap* and *Taz*, White et al. found that YAP/TAZ are required for the maintenance of *NF2*-deficient kidney cancer tumors in mice [38]. However, their sensitivity to pharmacologic YAP/TAZ-TEAD inhibitors has not yet been described.

Here, we report the identification and characterization of a novel covalent and irreversible YAP/TAZ-TEAD inhibitor, SWTX-143. We describe the direct binding of SWTX-143 to all TEAD isoforms at atomic resolution, as well as its selective transcriptional and phenotypic impact on various tumor models characterized by Hippo pathway alterations. We demonstrate a significant reversion of mesothelioma tumorigenesis and rescue of survival in a genetically induced orthotopic mesothelioma mouse model. Finally, SWTX-143 also potently reduced growth of *NF2*-mutant kidney cancer cell lines, indicating that the sensitivity of mesothelioma models to YAP/TAZ-TEAD inhibitors may be applicable to other Hippo-mutant tumor subsets.

MATERIALS AND METHODS

Cells lines

NCI-H226 (RRID:CVCL_1544), NCI-H2052 (RRID:CVCL_1518), NCI-H28 (RRID:CVCL_1555), HEK293 (RRID:CVCL_0045) and ACHN (RRID:CVCL_1067) were purchased from ATCC and UO31 (RRID:CVCL_1911) and SN12C (RRID:CVCL_1705) were acquired from NIH at the DCTD TUMOR REPOSITORY. Mutational data for each cell line was obtained from cBioportal.org.

Chemical reagents

Palbociclib and cisplatin were acquired at Tocris. Chemical synthesis and preparative chiral SFC (Supercritical Fluid Chromatography) of SWTX-143 is described in WO2022072741 (Cpd. No. 075, p. 224-225; analytical data: p. 291) [39]. Briefly, we used a Waters Thar SFC-80 instrument with a Chiralpak AD-H (5µm, 30x250 mm) column, CO_2 as the mobile phase, MeOH as the co-solvent at 30°C, and detection at 214nm. Elution was with 80% CO_2 and 20% EtOH, a flow of 60g/min, and 1500psi ABPR at 30°C.

Protein production

Human TEAD1-4 YAP binding domains were expressed as His-tagged proteins in BL21 (DE3) cells. After sonication in lysis buffer (50mM Tris HCl pH 7.5, 250mM NaCl, 10% glycerol, 10mM imidazole) TEADs were purified by affinity chromatography (IMAC-5mL FF). Proteins were eluted by imidazole, His-tags removed by thrombin cleavage by thrombin, and further purified by size exclusion chromatography (Superdex S75 16/60) in 20mM TrisHCl pH7.0; 150mM NaCl; 5% Glycerol; 2mM DTT. For crystallization, TEAD1 was concentrated to 10mg/ml. A 3-molar excess of compound SWTX-143 was added to the protein prior to crystallization trials.

Structure determination

TEAD1 crystals grew in drops (Mosquito robot SPT Labtech) at 22°C in 2M Ammonium sulfate. Data were collected on the PROXIMA-2 beamline at SOLEIL synchrotron (Saint-Aubin, France). Data were processed with autoPROC/stararaniso (GlobalPhasing), structures solved by molecular replacement with Phaser using an in-house structure of TEAD1 as search model, and refined by iterative cycles using

Buster, and manually fitted with Coot (RRID:SCR_014222). Model quality was monitored with Rampage.

Native mass spectrometry

TEAD stock solutions were desalted on Zeba columns against $AcONH_4$ 200mM pH7.5. Protein concentration was adjusted to 40µM in $AcONH_4$ 200mM pH7.5. When desired, Palmitoyl CoA was added (5eq, RT, 30 minutes), followed by desalting on Zeba columns. For native MS analysis, a final protein concentration of 10µM in 50mM $AcONH_4$ was used. Denaturing MS analysis was done at 1µM protein in ACN/H_2O/FA, 50/50/0.5 solution.

Calibration and data processing

Data were acquired on an ESI-TOF mass spectrometer (Micro mass LCT) using a Triversa Nanomate. Acquisitions and calibration were performed on the m/z range 500-5,000. A 2µM myoglobin solution (for denaturing MS) and a 2g/l cesium iodide in 2-propanol/water (50/50 v/v) (for native MS) were used as external calibrants. Quantification of the different species was based on the intensity (peak height) of the two major charge states (9+ and 8+) following the two equations.

$$(\%)\boldsymbol{PL} = \frac{\mathbf{I(PL)9+ + I(PL)8+}}{\mathbf{I(P + PL + PPalm)9+ + I(P + PL + PPalm)8+}}$$

$$(\%)\boldsymbol{PPalmL} = \frac{\mathbf{I(PPalmL)9+ + I(PPalmL)8+}}{\mathbf{I(PPalm + PPalmL)9+ + I(PPalmL + PPalm)8+}}$$

(%)PL: binding proportion on protein, *(%)PPalm:* binding proportion on palmitoylated protein, *I:* Intensity, *PL:* Protein bound to Ligand

Data interpretation was performed using MassLynx v4.1 software (Waters, RRID:SCR_014271) and masses were calculated using the peak picking method. Since the molecular isotopic cluster was not fully resolved, average molecular masses were measured.

Thermal Shift Assays

Thermal shift assays were performed using the StepOnePlus Real-Time PCR System (Applied Biosystems). Compound predilutions were made to maintain an equal percentage of DMSO. The 4 TEAD proteins were incubated with compound for 30 minutes at room temperature in 25mM HEPES, 150mM NaCl, pH 7.5 buffer and analyzed according to the Applied Biosystems protocol.

Reporter Gene Assays

HEK293 cells were transiently transfected with the 8xGTIIC TEAD luciferase reporter (RRID:Addgene_34615) using JetPEI (Polyplus) and plated with pre-diluted compounds. Luciferase levels were measured after 24 hours using Perkin Elmer SteadyLite substrate on an Envision reader (PerkinElmer). The ability of a test compound to inhibit this activity was determined as: Percentage inhibition = [1-((RLU with vehicle – RLU with test compound) divided by (RLU with vehicle – RLU with positive control inhibitor))] * 100.

Cell number, cell cycle, and cell death assays

Cell lines were seeded, medium with compound was added after the next day (day 1), and cell numbers were determined with ATPLite (Perkin Elmer, 6016943) on day 6. Cell numbers for proliferation assays were measured with CellTiterGlo. The Click-iT™ EdU proliferation assay (ThermoFisher scientific, # C10499) was applied to NCI-H226 cells that were seeded at 1500 cells/96-well plate well and incubated overnight. Active Caspase3/7 were detected using the Caspase-Glo assay (Promega, G8091) on NCI-NCI-H226 cells that were incubated overnight with compounds.

RNA extraction & Transcriptional Profiling

NCI-H226 and ACHN cells were seeded at 600,000 cells per well and incubated with SWTX-143 overnight (100nM). RNA was extracted using RNeasy Kit (Qiagen, #74004), treated with DNase (Qiagen, #79254) and stored at -80ºC. Samples were sequenced at BGI (Shenzhen, Guangdong, China). mRNA fragments were purified, used for cDNA library preparation, and analyzed through the BGISEQ-500 platform (RRID:SCR_017979). Quality control and sequence trimming was done with FastQC and Cutadapt followed by mapping to the human genome (GRCh37, hg19) using STAR (RRID:SCR_004463). After filtering lowly expressed genes (<1 cpm),

differential gene expression analysis was performed using the DESeq2 R-package (RRID:SCR_000154). Genes were considered significantly downregulated, when adjusted p values were < 0.05 and log2 fold changes were < -0.6. Heatmaps show row-normalized log2 scale expressions as obtained by 'regularized log' transformation from DESeq2 Gene Set Enrichment Analysis (GSEA) was performed by the GSEA algorithm using clusterProfiler and visualized using enrichplot (RRID:SCR_003199). The motif enrichment analysis was done using i-CisTarget [40] with default settings. The YAP signature was from [31]. The RNAseq data can be accessed by GSE222963.

Formulation and PK analysis

SWTX-143 was formulated in PEG-400 40%, 1,2-Propanediol 30% and H_2O 30% and dosed orally (PO) at the indicated concentrations. Bioanalysis of SWTX-143 in plasma was determined using standard LC-MS/MS procedures.

In vivo xenografts and RNA-seq

10x10E6 NCI-H226 cells in 0.2ml PBS mixed with 1:1 Matrigel (Corning Inc) were subcutaneously inoculated into the flank of female BALB/c nude mice (RRID:IMSR_ORNL:IE-BALB/c). Mice were randomized when the mean tumor volume reached approximately 170 mm^3 based on “Matched distribution” method using tumor volumes (StudyDirectorTM software, version 3.1.399.19). Tumor volumes were measured twice per week and calculated using the formula: “V = (L x W x W)/2, with L = tumor length (mm) and W = tumor width (longest dimension perpendicular to L). Mice were monitored daily and sacrificed when the humane endpoint was reached according to the national guidelines (tumor volume >3000 mm^3 or >20% body weight loss relative to the weight at the start).

Genetic mesothelioma model

Lats1$^{fl/fl}$; *Lats2*$^{fl/fl}$ [41] were crossed to *p53*$^{fl/fl}$ mice [42] to produce *p53*$^{fl/fl}$;*Lats1*$^{fl/fl}$;*Lats2*$^{fl/fl}$ mice. SWTX-143 was administered at 30mg/ml via gavage twice daily for two weeks. Adult mice were sedated with Ketamine:Xylazine solution and 10^8 Adeno-Cre virus particles (VectorBiolabs dE1/E3, #1700) were injected intrapleurally by fixing mice on their back and inserting the needle between the ribs through the chest wall [43]. All mouse experiments were approved by the institutional ethical commission at KU

Leuven and performed in accordance with relevant institutional and national guidelines and regulations.

Lung histology and immunofluorescence

Mouse lungs were fixed in 4% paraformaldehyde (VWR) in 1xPBS for 48 hours at 4ºC, embedded in paraffin and cut (5µm) using a microtome. Paraffin sections were stained with hematoxylin and eosin (H&E) and imaged on a Axio Scan.Z1 slide scanner. For immunofluorescence staining, samples were dewaxed, rehydrated in several steps, permeabilized, blocked for 2h in 3% bovine serum albumin (BSA) at room temperature, and incubated overnight with primary antibodies (WT1 (RRID:AB_2043201); Mesothelin (RRID:AB_1279130); Vimentin (RRID:AB_10695459). The following day, samples were washed in PBS, incubated in secondary antibody solution for 1h at room temperature (Cy3-conjugated donkey anti-rabbit IgG, Jackson, (RRID:AB_2313568), Cy3-conjugated donkey anti-rat IgG, (RRID:AB_2340669) and 488-conjugated donkey anti-rabbit, (RRID:AB_2313584), and mounted in Mowiol (Sigma), and scanned on an Olympus FV1200 confocal microscope. The immunofluorescent stainings were analyzed to determine mesothelial layer thickness and to confirm cell fate using the mesothelin stainings at high magnification (40 and 60x objectives).

Quantifications and statistics

ImageJ software was used for quantifications (RRID:SCR_003070). Mesothelioma cell layer thickness was quantified on H&E stainings by measuring the distance from the basal membrane to the edge of the mesothelium at multiple points regularly distributed around the perimeter of the section. These data are presented as the mean +/- SEM and groups were tested for significant differences using unpaired t-tests in which a p value of 0,05 was considered statistically significant.

RESULTS

Identification of SWTX-143 as a pan-TEAD palmitoylation-pocket binder

To identify compounds that bind to the palmitoylation pocket (P-pocket) of TEADs, we initiated a structure-based drug design approach using the publicly available structural information at the time (Apo-TEAD2 and TEAD2 in complex with ligands such as flufenamic acid [44] and myristic acid [28]). A native mass-spectrometry (MS) assay was established to determine binding of compounds to the P-pocket of TEAD1. Upon purification from bacteria, the YAP-binding domain of TEAD1 (TEAD1$^{R209\text{-}D426}$) is typically moderately palmitoylated (up to 15%) but can be fully covalently palmitoylated using palmitoyl CoA (detected by MS shift of 236 Da). We thus determined the extent and specificity of compound binding to the P-pocket by comparing the percentage of binding to the native (poorly palmitoylated) versus the fully palmitoylated protein using native MS. Several iterative cycles of medicinal chemistry to optimize selective TEAD P-pocket binders led to the identification of SWTX-143 (**Fig. 1A**; medicinal chemistry optimization to be described in detail elsewhere) [39]. SWTX-143 binds to native TEAD1 (67% and 92% binding at 5µM and 20µM respectively) but did not bind to the fully palmitoylated TEAD1 protein (0% and 9% binding at 5µM and 20µM respectively), indicating that SWTX-143 exclusively binds into the P-pocket of TEAD1 (**Fig. 1B** and **1C**). An MS-based assay under denaturing conditions further demonstrated that SWTX-143 covalently bound to TEAD1 protein at 20µM, consistent with the presence of an acrylamide electrophile in the molecule (**Fig. 1D**).

To elucidate the binding mode of SWTX-143 to TEAD1 at atomic resolution, we soaked SWTX-143 into crystals of TEAD1$^{R209\text{-}D426}$. X-Ray data collection of the complex to a resolution of 1.6Å and crystallographic structure refinement showed that SWTX-143 occupied up to 80% of the volume of the P-pocket and that it binds in an orientation suitable to form a covalent bond with Cys359 via its acrylamide function (**Fig. 1E)**.

To determine whether SWTX-143 can bind to all 4 members of the TEAD family, Thermal Shift Assays were performed on the YAP-binding domains of the 4 TEAD isoforms (TEAD1$^{R209\text{-}D426}$, TEAD2$^{A217\text{-}D447}$, TEAD3$^{R218\text{-}D435}$, TEAD4$^{S217\text{-}E434}$). When co-incubating SWTX-143 (10µM) with the TEAD protein domains, a significant thermal stabilization was observed for all four TEAD isoforms (ranging from 3 to 9°C),

demonstrating that SWTX-143 is a pan-TEAD binder (**Fig. 1F**). Interestingly, the modest binding of the SWTX-143 racemic mixture to TEAD3 was due to the lack of TEAD3 binding to one of the enantiomers, SWTX-143-A, which did not stabilize TEAD3 under the conditions tested, whereas the alternate enantiomer, SWTX-143-B, clearly bound to TEAD3 (stabilization of 3.78°C) (**Fig. 1F**). These data show that subtle conformational differences between compounds can impact TEAD isoform binding preference, despite the highly conserved nature of the P-pocket across all isoforms.

SWTX-143 is a potent, irreversible, and selective inhibitor of YAP/TAZ-TEAD transcription

Auto-palmitoylation of TEAD proteins impacts YAP/TAZ-TEAD complex formation and stability[27,28]. To investigate the impact of our TEAD P-pocket binders on TEAD transcriptional activity, we tested SWTX-143, along with the pure enantiomers, SWTX-143-A and SWTX-143-B, in HEK293 cells transiently transfected with a TEAD-reporter construct that expressed firefly luciferase under the control of 8 repeats of a TEAD responsive element [45]. SWTX-143 potently repressed luciferase expression from the TEAD-reporter (IC_{50} = 12nM) while not affecting the viability of HEK293 cells (**Fig. 2A**). No significant differences between the enantiomers of SWTX-143 were observed indicating that TEAD3 does not significantly contribute to YAP/TAZ-TEAD transcriptional output in this assay consistent with its low expression levels (**Fig. 2B**). Moreover, the action of SWTX-143 was selective as it did not affect luciferase expression driven by a HIF responsive element (HRE) (**Fig. 2B**).

Because we demonstrated covalent binding of SWTX-143 to TEAD1 protein, we examined the reversibility of TEAD transcriptional inhibition by SWTX-143 in this cellular reporter system. HEK293 cells were transiently transfected with the TEAD-reporter construct and incubated for 3, 6, 12 or 24 hours with SWTX-143, after which the compound-containing medium was removed and replaced with medium for a total period of 24 hours when reporter activity was measured (**Fig. 2C**). Incubation of the transfected cells for as short as 3 hours with SWTX-143, followed by a wash-out period of 21 hours, effectively reduced transcriptional reporter activity (IC_{50} = 95nM), consistent with a fast and irreversible mechanism of action of SWTX-143. Longer incubation for 6, 12 or 24 hours still moderately increased the potency of transcriptional repression (IC_{50} = 58, 34 and 16nM, respectively), as expected for a reactive covalent

inhibitor. Thus, a short exposure of tumor cells to SWTX-143 may be sufficient to evoke a long-lasting transcriptional impact.

To determine the specificity of SWTX-143 on gene expression in more detail, we turned to the Hippo pathway inactivated (*NF2*-deficient) mesothelioma cell line, NCI-H226. We measured the impact of 100nM SWTX-143 on the whole transcriptome of this cell line by RNA-sequencing after 6 hours of compound incubation. Differential expression analysis identified 327 downregulated and 380 upregulated genes after SWTX-143 treatment compared to vehicle treatment (adjusted p-value < 0.05; log2FC > 0.6). A YAP signature was strongly repressed by SWTX-143 (**Fig. 2D** and **2E**) [31], but the transcriptional output of most other signaling pathways was not strongly affected (**Fig. 2F**). To further investigate the regulation of the downregulated genes, we employed iCis-target to identify transcription factor binding motifs that were enriched in the 20kb genomic region surrounding their transcription start site [40]. This identified binding sites for TEAD factors as the top hit with a high enrichment score (NES=8.3) and binding sites for E2F family members as the only other enriched motifs (NES=6.54) (**Fig. 2G**). Strikingly, 80% of the downregulated genes (262 of 327 genes) had TEAD binding sites, indicating they could be direct targets of TEAD factors (**Fig. 2H** and **2I**). Altogether, these data demonstrate that SWTX-143 represses YAP/TAZ-TEAD transcriptional activity in a selective manner.

SWTX-143 inhibits the proliferation of Hippo pathway-mutant cancer cell lines

Malignant pleural mesothelioma exhibits recurrent genetic alterations in *NF2* and *LATS2*, resulting in constitutive YAP/TAZ activity [13–15]. Here, we tested the impact of SWTX-143 on the proliferation of three distinct mesothelioma cancer cell lines that are characterized by and depend on loss-of-function alterations in *NF2* (Mero-14, NCI-H226 and NCI-H2052)(**Fig. S1A**) and one that is deficient in *LATS1* and *LATS2* (MSTO-211H). Strikingly, proliferation of all four cell lines was highly sensitive to SWTX-143 (IC_{50} ranging between 5 and 207nM) (**Fig. 3A** and **3B**). On the other hand, SWTX-143 treatment only modestly impacted the proliferation of the NCI-H28 and NCI-H2452 mesothelioma, HeLa, SiHa and CaSki cancer cell lines which lack genetic alterations in known Hippo pathway components (Hippo-WT) (**Fig. 3A, 3B** and **S1B**).

To decipher the mechanism responsible for the observed decrease in cell number over time in Hippo-mutant mesothelioma cell lines, we distinguished whether SWTX-143 was cytotoxic (inducing apoptosis) or cytostatic (promoting cell cycle arrest). SWTX-143 did not promote apoptosis in the *NF2*-deficient mesothelioma cell line NCI-H226, in contrast to cisplatin (**Fig. 3C**). Rather, SWTX-143 induced cell cycle arrest with similar kinetics as the CDK4/6 inhibitor palbociclib, as shown by a strong reduction of EdU-positive cells over time (**Fig. 3D**). Thus, SWTX-143 acts by inhibiting the proliferation of Hippo mutant mesothelioma cells in vitro.

In addition to mesothelioma, a subset of kidney cancers exhibits frequent mutations in Hippo pathway genes. We thus investigated the response of a small panel of kidney cancer cell lines to SWTX-143 and its enantiomers (**Fig. 3E** and **3F**). Interestingly, cell lines carrying mutations in Hippo pathway components (SN12C *NF2*^{LOF}, UO31 *LATS2*^{A324V} and ACHN *NF2*^{R57*}/*LATS2*^{LOF}) were particularly sensitive to SWTX-143 incubation, whereas the proliferation of HEK293 kidney cells (Hippo-WT) was not affected by SWTX-143. Like the specificity of SWTX-143 action in NCI-H226 mesothelioma cells, we observed robust downregulation of canonical YAP/TAZ-TEAD target genes and the YAP signature by SWTX-143 treatment of ACHN kidney cancer cells (NES = -2.19, P = 8.14e-08) (**Fig. S2A&B**).

Finally, we compared the efficacy of SWTX-143 to the efficacy of the previously identified TEAD P-pocket binders K-975 and VT104 in the TEAD and HIF1 reporter gene assays and the mesothelioma proliferation assays (**Fig. 3G**). This showed that SWTX-143 was equally effective in suppressing TEAD transcriptional activity but had higher efficacy in inhibiting the proliferation of mesothelioma cells with lower toxicity in HEK293 and H28 cells compared to K-975 and VT104.

SWTX-143 causes regression of *NF2*-deficient human mesothelioma xenografts

SWTX-143 was optimized to be suitable for oral administration and to have sufficient plasma exposure allowing animal testing (oral bioavailability ≥75% and half-life of about 2 hours). We thus evaluated the efficacy of SWTX-143 in a human mesothelioma xenograft mouse model. We subcutaneously injected NCI-H226 cells and when tumors reached about 170mm^3, mice were randomized into groups and treated once daily with SWTX-143 (10, 25 and 50mg/kg) or vehicle for 19 days.

Although administration of SWTX-143 had little effect on tumor volume during the first week of dosing, a clear dose-dependent tumor regression was observed during the two subsequent weeks of dosing (**Fig. 4A**). Significant anti-tumor efficacy was observed at the end of the 18 days of compound administration for all dosing regimens (**Fig. 4B**). Notably, none of the treatments resulted in overt toxicity or loss of body weight of the mice (**Fig. 4C**). Thus, SWTX-143 treatment causes strong regression of mesothelioma tumors in vivo without significant secondary adverse effects.

To corroborate that these anti-tumor effects were driven by inhibition of YAP/TAZ-TEAD-driven transcription in the tumor, we analyzed tumor gene expression profiles by RNA-seq. Indeed, increasing doses of SWTX-143 (resulting in dose-proportional increases of plasma exposure) correlated with stronger repression of YAP/TAZ-TEAD target genes in tumors, measured at the endpoint of the study (**Fig. 4D&S3**). Notably, although SWTX-143 plasma exposure was transient (**Fig. 4E**), it was sufficient to trigger a sustained repression of YAP/TAZ-TEAD target genes after 4 and 24 hours after the last dose of SWTX-143 (**Fig. 4D**), probably due to irreversible covalent binding of the compound to the TEAD complex. These results show that SWTX-143 treatment causes a strong and specific inhibition of YAP/TAZ-TEAD target gene expression in vivo.

Genetically induced mouse mesothelioma regresses upon SWTX-143 treatment

Next, we investigated the efficacy of SWTX-143 on an orthotopic mesothelioma mouse model that was generated by conditionally deleting *p53, Lats1* and *Lats2* in mesothelial cells of adult mice. An adenovirus that constitutively expressed Cre (adeno-Cre) was injected into the pleural cavity of $p53^{fl/fl}$; $Lats1^{fl/fl}$; $Lats2^{fl/fl}$ mice (**Fig. 5A**). This virus efficiently infected mesothelial cells, which normally form a single cell layer covering the pleural cavity and triggered massive mesothelial cell proliferation that developed into a thick layer of ectopic mesothelial cells after 2 weeks (Fig. 5B). These cells expressed the mesothelioma markers WT1, Mesothelin, and Vimentin, which are used in the clinic to diagnose mesothelioma (**Fig. 5B&S4A**)[46]. Soon after these two weeks, mutant mice needed to be sacrificed due to labored breathing (**Fig. 5C**). Mutant mice also had ectopic proliferation of pericardial cells surrounding the heart, while other organs that do not reside in the pleural cavity such as the liver were not affected. Mutant mice were then treated with SWTX-143 or vehicle starting two weeks after

adeno-Cre injection when they already had advanced mesothelioma and were just a few days before they would normally have had to be sacrificed. Vehicle treatment did not affect mesothelioma progression and mice had to be sacrificed 2-4 days after the start of treatment (**Fig. 5D**). In contrast, SWTX-143-treated mice had normal breathing within a few days after the start of treatment and survived until the termination of the experiment after 2 weeks of treatment (**Fig. 5D**).

We then quantified the thickness of the mesothelial cell layer on Hematoxylin and Eosin (H&E) stained lung sections and measured the distance from the basal membrane to the edge of the mesothelium at multiple points around the perimeter of the section. At the start of treatment and after a few days of vehicle treatment, the lungs of *p53;Lats1;Lats2* triple mutant mice showed a massive expansion of the mesothelial layer from a 30-50μm thick single cell layer, to a large, over 400μm thick layer of about 10 cells stacked on top of each other (**Fig. 5B** and **5D**). This mesothelial overgrowth dramatically regressed in SWTX-143-treated mice to an average thickness of 80μm that appeared to be normal with a single cell layer around most of the lung surface (**Fig. 5D**). A few areas still had multiple layers of cells, however, these regions displayed many bloated and necrotic cells, and cells that were detaching from the tissue (**Fig. S4B**). These observations were confirmed by specifically detecting mesothelial cells by WT1 antibody staining (**Fig. 5B**, right panels). We conclude that SWTX-143 treatment potently caused mesothelioma regression in this orthotopic *in vivo* mesothelioma model.

DISCUSSION

The Hippo pathway is an important target for drug discovery since constitutive activation of YAP/TAZ by genetic and non-genetic dysregulation occurs across multiple hard-to-treat solid tumor types and is associated with treatment resistance [1–6]. As the TEAD proteins are the main partner transcription factors of YAP/TAZ, targeting the TEAD transcription factors is emerging as a promising therapeutic strategy to treat Hippo-inactivated tumors [3–5]. Here, we provide preclinical evidence that direct covalent TEAD P-pocket engagement is remarkably effective to treat mesothelioma, a prime example of a Hippo-mutant cancer. Using a novel, potent and selective pan-TEAD inhibitor, SWTX-143, we demonstrate tumor regression of subcutaneously implanted human mesothelioma cells, and more importantly, near complete normalization of orthotopic mouse mesothelioma and full rescue of survival in a newly developed genetic model. In these mouse studies, we did not observe any overt signs of tolerability alerts, even though YAP/TAZ-TEAD transcription in tumors was profoundly suppressed. More extensive tolerability studies are needed, but this analysis suggests that a therapeutic index can be achieved using this mechanism of YAP/TAZ-TEAD inhibition. Of note, a potential advantage of a covalent irreversible TEAD binder, such as SWTX-143, is the limited systemic exposure needed to achieve long-term sustained target engagement in tumors and efficacy. On the other hand, covalent Cys binders may have the downside of being susceptible to resistance by mutation of this residue, as has been clinically observed for covalent kinase inhibitors such as ibrutinib for example [47]. Importantly however, the Cys residue targeted by SWTX-143 (Cys 359 in TEAD1) is autopalmitoylated and important for TEAD functionality which decreases the risk of resistance through mutation of this Cys as this would directly impair the activity of the mutant TEAD protein.

Despite the impressive tumor regression in distinct mouse cancer models *in vivo*, we did not observe killing of mesothelioma cancer cells by SWTX-143 *in vitro*. We speculate that YAP/TAZ-TEAD inhibition leads to more impressive tumor cell killing *in vivo* due to its impact on cell-cell and/or cell-matrix interactions, processes that are abnormal in cells cultured on artificial surfaces, which may make them less vulnerable to YAP/TAZ-TEAD inhibition. A better understanding of the precise mechanism of action of YAP/TAZ-TEAD inhibitors may also lead to rationally selected combination regimens. Recently, a detailed analysis of clinical pleural mesothelioma datasets

demonstrated that YAP/TAZ transcriptional markers tracks with worse outcome [48]. Further, loss of NF2 increases tumorigenicity in mesothelioma cells. The data reported here support a clinical stratification strategy for TEAD inhibitors based on YAP/TAZ transcriptional activation and/or loss of NF2. However, further (clinical) research is required to determine what the most optimal predictive biomarker would be to guide patient stratification. Finally, we provided evidence that the efficacy observed with YAP/TAZ-TEAD inhibitors is not limited to mesothelioma models but may be extended to other tumor types with Hippo-pathway alterations such as kidney cancer.

FIGURE LEGENDS

Figure 1: Identification of SWTX-143 as a pan-TEAD palmitoylation-pocket binder. A) Chemical structure of SWTX-143. The star indicates the chiral center. **B,C)** Native mass spectroscopy (MS) zoomed in on the 9+ charged state of TEAD1 to detect binding of SWTX-143 to the palmitoylation pocket of TEAD1$^{R209\text{-}D426}$. Spectra of native (B) and fully palmitoylated (C) TEAD after incubation with palmitoyl-CoA. **D)** Denaturing MS to measure covalent binding of SWTX-143 to TEAD1. **E)** Crystal structure of SWTX-143 in the P-pocket of TEAD1. Amino acids important for the binding are highlighted. **F)** Measurements from Thermal Stability Assays of SWTX-143 binding to the TEAD1-4 isoforms.

Figure 2: SWTX-143 is a potent and selective YAP/TAZ-TEAD transcriptional inhibitor. A) Reporter gene assays upon SWTX-143 treatment using the TEAD reporter 8xGTIIC and a Hif1 reporter (HRE) in HEK293 cells. **B)** IC_{50} values of reporter gene assays upon treatment with SWTX-143 and its 2 enantiomers. **C)** Reporter gene assays with different SWTX-143 incubation times and wash-out periods. **D)** Expression of YAP signature genes in vehicle and SWTX-143 treated NCI-H226 cells. **E)** Gene Set Enrichment Analysis of YAP signature. **F)** Heatmap of differential pathway analysis comparing vehicle and SWTX-143 treated NCI-H226 cells. **G)** TEAD binding motives identified by iCis target. **H)** Venn diagram showing the proportion of TEAD target genes among all downregulated genes upon SWTX-143 treatment. **I)** Volcano plot of the differential gene expression analysis of SWTX-143 vs vehicle. TEAD target genes are marked in green.

Figure 3: SWTX-143 inhibits the proliferation of Hippo-mutated cancer cell lines. A,B) Cell numbers of different *Hippo*-mutant mesothelioma cell lines and the Hippo-WT control lines H28, HeLa and Siha upon SWTX-143 treatment over 6 days. IC_{50} values are shown in the tables. *H2452 data displayed in Fig. S1B. **C)** Caspase3/7 activity assay in NCI-H226 cells showing luminescence measurements (RLU). Cisplatin served as a positive control. **D)** Number of EdU-positive NCI-H226 cells upon different treatments (Palbociclib, SWTX-143). **E)** Cell numbers of Hippo-mutant and Hippo-WT kidney cell lines and IC_{50} values presented in the table (**F**). (**G**) Summary of results comparing SWTX-143 to published compounds K-975 and VT104. NT, not tested.

Figure 4: SWTX-143 inhibits the growth of Hippo-mutant human mesothelioma xenografts. A) Tumor volume over time of NCI-H226 xenograft tumors in mice treated with SWTX-143 or vehicle (8 mice/group). Values are average ± SEM. **B)** Body weight of NCI-H226 tumor-bearing mice during SWTX-143 and vehicle treatment. Values are average ± SEM. Error bars are too small to be visible. **C)** Tumor volume at 18 days of treatment. **D)** Heatmap showing YAP signature genes in vehicle- and SWTX-143-treated NCI-H226 tumor-bearing mice. **E)** SWTX-143 plasma exposure at the indicated doses and time points during experiment in **D**).

Figure 5: SWTX-143 treatment triggers tumor regression in genetically induced mesothelioma. A) Experimental setup. 2 weeks after injection of adeno-Cre, vehicle and SWTX-143 were administered to mice for 2 weeks. **B)** Lungs from a normal mouse, and mutant mice at start of treatment, vehicle-treated for 2 days, and SWTX-143-treated for 2 weeks. Left two panels are overviews and zoom-ins of H&E-stained lungs; right two panels are immunofluorescent pictures of lung sections stained for WT1 (mesothelial marker, red/grey) and DAPI (nuclei, blue). **C)** Kaplan-Meier curves of vehicle and SWTX-143-treated mice. Survival curves were compared using log-rank (Mantel-Cox) test (p= 0.0008). **D)** Quantification of mesothelial layer thickness. **: p=0.008.

Figure S1: SWTX-143 does not affect *Hippo*-wild type mesothelioma cells. A) Fraction of transfected cells after re-expression of NF2 in HEK293 and *NF2*-mutant mesothelioma cell lines. The proliferation of *NF2*-mutant mesothelioma cell lines, but not the NF2 wild-type HEK293 cells, is suppressed by NF2 overexpression. **B)** Effect of SWTX-143 on the proliferation of the *Hippo*-wild type mesothelioma cell line H2062.

Figure S2: SWTX-143 is a selective YAP/TAZ-TEAD transcriptional inhibitor in the NF2 deficient kidney cancer cell line ACHN. A) Heatmap showing YAP signature genes in vehicle and SWTX-143-treated kidney cancer cell line. **B)** Gene Set Enrichment Analysis of the YAP signature.

Figure S3: Pathway analysis of tumors on SWTX-143 treatment. Heatmap of differential pathway analysis comparing the tumors of vehicle and SWTX-143-treated mice.

Figure S4: Mesothelioma regression upon SWTX-143 treatment. A) Immunofluorescence stainings of lung sections from mice with mesothelioma after 2 weeks after Adeno-Cre injection, stained for Vimentin (green) and Mesothelin (red). **B)** Picture of an H&E staining of a lung section from a mouse with mesothelioma that was treated with SWTX-143 for one week.

ACKNOWLEDGMENTS

We are grateful for excellent technical support from Marianne Croonenborghs (Cistim Leuven), Merja Bhailal Chakubhai (Aragen) and Tao Yang (Crownbio). We thank Randy Johnson and Chris Marine for sending mouse strains. This work was supported by grants from Stichting tegen Kanker to G.H.

AUTHOR'S CONTRIBUTIONS

H.H., A.C., B.V., W.S., S.S., L.S., E.K., M.N, E.S., W.H, H.K, A.M., L.V.H., L.S., F.C., F.D. conducted experiments. W.K. conducted bioinformatics analysis. H.H., A.C., M.V., A.M., P.C., S.G., G.H. designed the study. H.H., A.C., M.V. and G.H. wrote the manuscript and all authors reviewed and edited the manuscript.

SUPPLEMENTAL INFORMATION

Figure S1

Figure S2

Figure S3

Figure S4

X-ray specifications

Supplemental methods: X-ray specifications

Data processing	
Crystal	TEAD1-CIM205143
Wavelength (Å)	0.9801
Space group	P212121
Cell dimensions	
a, b, c (Å)	36.6 89.7 136.3
α, β, γ (°)	90, 90, 90
Resolution (last shell) (Å)	74.94-1.58 (1.81-1.58)
Unique Reflections (last shell)	34809 (1738)
Completeness (last shell) (%)	84.0 (45.0)
Redundancy (last shell)	5.2 (5.0)
I/ σ(I) (last shell)	8.7 (1.7)
R_{pim} (last shell) (%)	6.5 (57.0)
CC(1/2) (last shell)	0.997 (0.566)
Structure Refinement	
R_{cryst} (%)	20.84
R_{free} (%)	25.93
Number of atoms	
Protein (chain A)	1827
Ligand (chain A)	26
Protein (chain B)	1856
Ligand (chain B)	26
Water molecules	288
R.m.s. deviations	
Bond lengths (Å)	0.010
Bond angles (°)	1.110
Average B factor (Å^2)	
Protein (chain A)	21.28
Ligand (chain A)	19.20
Protein (chain B)	23.44
Ligand (chain B)	21.40
Water molecules	38.28
Ramachandran plot (%)	
Favored	97.8
Additional	2.2
Disallowed	0

REFERENCES

1. Harvey, K. F., Zhang, X. & Thomas, D. M. The Hippo pathway and human cancer. *Nat. Rev. Cancer* **13**, 246–257 (2013).
2. Varelas, X. The hippo pathway effectors TAZ and YAP in development, homeostasis and disease. *Dev.* **141**, 1614–1626 (2014).
3. Dey, A., Varelas, X. & Guan, K. L. Targeting the Hippo pathway in cancer, fibrosis, wound healing and regenerative medicine. *Nat. Rev. Drug Discov.* **19**, 480–494 (2020).
4. Zanconato, F. *et al.* YAP/TAZ as therapeutic targets in cancer. *Curr. Opin. Pharmacol.* **29**, 26–33 (2016).
5. Zheng, Y. & Pan, D. The Hippo Signaling Pathway in Development and Disease. *Dev. Cell* **50**, 264–282 (2019).
6. Johnson, R. & Halder, G. The two faces of Hippo: targeting the Hippo pathway for regenerative medicine and cancer treatment. *Nat. Rev. Drug Discov.* **13**, 63–79 (2014).
7. Verboven, E. *et al.* Regeneration Defects in Yap and Taz Mutant Mouse Livers are Caused by Bile Duct Disruption and Cholestasis. *Gastroenterology* **160**, 847–862 (2020).
8. Azzolin, L. *et al.* YAP/TAZ Incorporation in the b-Catenin Destruction Complex Orchestrates the Wnt Response. *Cell* **158**, 157–170 (2014).
9. Ivan M Moya and Georg Halder. The Hippo pathway in cellular reprogramming and regeneration of different organs. *Curr. Opin. Cell Biol.* **43**, 62–68 (2016).
10. Piccolo, S., Panciera, T., Contessotto, P. & Cordenonsi, M. YAP/TAZ as master regulators in cancer: modulation, function and therapeutic approaches. *Nat. Cancer* **4**, 9–26 (2022).
11. Thompson, B. J. YAP/TAZ: Drivers of Tumor Growth, Metastasis, and Resistance to Therapy. *BioEssays* **42**, 1900162 (2020).
12. Zhang, W. Q. *et al.* Targeting YAP in malignant pleural mesothelioma. *J. Cell. Mol. Med.* **21**, 2663–2676 (2017).
13. Bueno, R. *et al.* Comprehensive genomic analysis of malignant pleural mesothelioma identifies recurrent mutations, gene fusions and splicing alterations. *Nat. Genet.* **48**, 407–416 (2016).
14. Cheung, M., Menges, C. W. & Testa, J. R. Germline and Somatic Mutations in Human Mesothelioma and Lessons from Asbestos-Exposed Genetically Engineered Mouse Models. *Curr. Cancer Res.* **978-3-319-**, 175–195 (2017).
15. Xu, D., Yang, H., Schmid, R. A. & Peng, R. W. Therapeutic Landscape of Malignant Pleural Mesothelioma: Collateral Vulnerabilities and Evolutionary Dependencies in the

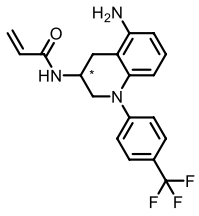
Spotlight. *Front. Oncol.* **10**, 1–14 (2020).
16. Rehrauer, H. *et al.* How asbestos drives the tissue towards tumors: YAP activation, macrophage and mesothelial precursor recruitment, RNA editing, and somatic mutations. *Oncogene* **37**, 2645–2659 (2018).
17. Janes, S. M., Alrifai, D. & Fennell, D. A. Perspectives on the Treatment of Malignant Pleural Mesothelioma. *N. Engl. J. Med.* **385**, 1207–1218 (2021).
18. Calvet, L. *et al.* YAP1 is essential for malignant mesothelioma tumor maintenance. *BMC Cancer* **22**, 1–14 (2022).
19. Luo, M. *et al.* Advances of targeting the YAP/TAZ-TEAD complex in the hippo pathway for the treatment of cancers. *Eur. J. Med. Chem.* **244**, 114847 (2022).
20. Kaneda, A., Seike, T., Danjo, T., Nakajima, T. & Otsubo, N. The novel potent TEAD inhibitor , K-975 , inhibits YAP1 / TAZ-TEAD protein-protein interactions and exerts an anti-tumor effect on malignant pleural mesothelioma. **10**, 4399–4415 (2020).
21. Tang, T. T. *et al.* Small molecule inhibitors of TEAD auto-palmitoylation selectively inhibit proliferation and tumor growth of NF2-deficient mesothelioma. *Mol. Cancer Ther.* **20**, 986–998 (2021).
22. Sun, Y. *et al.* Pharmacological blockade of TEAD-YAP reveals its therapeutic limitation in cancer cells. *Nat. Commun.* **13**, 6744 (2022).
23. Fan, A. M. *et al.* Covalent Disruptor of YAP-TEAD Association Suppresses Defective Hippo Signaling. *Elife* (2022).
24. Pobbati, A. V. & Hong, W. A combat with the YAP/TAZ-TEAD oncoproteins for cancer therapy. *Theranostics* **10**, 3622–3635 (2020).
25. Pobbati, A. V *et al.* Targeting the Central Pocket in Human Transcription Factor TEAD as a Potential Cancer Therapeutic Strategy. *Struct. Des.* **23**, 2076–2086 (2015).
26. Kristal Kaan, H. Y. *et al.* Crystal structure of TAZ-TEAD complex reveals a distinct interaction mode from that of YAP-TEAD complex. *Sci. Rep.* **7**, 1–11 (2017).
27. Noland, C. L. *et al.* Palmitoylation of TEAD Transcription Factors Is Required for Their Stability and Function in Hippo Pathway Signaling. *Structure* **24**, 179–186 (2016).
28. Chan, P. *et al.* Autopalmitoylation of TEAD proteins regulates transcriptional output of the hippo pathway. *Nat. Chem. Biol.* **12**, 282–291 (2016).
29. Mesrouze, Y. *et al.* Effect of the acylation of TEAD4 on its interaction with co-activators YAP and TAZ. *Protein Sci.* **26**, 2399–2409 (2017).
30. Mesrouze, Y. *et al.* The role of lysine palmitoylation/myristoylation in the function of the TEAD transcription factors. *Sci. Rep.* **12**, 1–8 (2022).
31. Wang, Y. *et al.* Comprehensive Molecular Characterization of the Hippo Signaling Pathway in Cancer. *Cell Rep.* **25**, 1304-1317.e5 (2018).
32. Dalgliesh, G. L. *et al.* Systematic sequencing of renal carcinoma reveals inactivation

of histone modifying genes. *Nature* **463**, 360–363 (2010).

33. Malouf, G. G. *et al.* Genomic Characterization of Renal Cell Carcinoma with Sarcomatoid Dedifferentiation Pinpoints Recurrent Genomic Alterations. *Eur. Urol.* **70**, 348–357 (2016).
34. Comprehensive Molecular Characterization of Papillary Renal-Cell Carcinoma. *N. Engl. J. Med.* **374**, 135–145 (2016).
35. Pal, S. K. *et al.* Characterization of Clinical Cases of Advanced Papillary Renal Cell Carcinoma via Comprehensive Genomic Profiling. *Eur. Urol.* **73**, 71–78 (2018).
36. Sourbier, C. *et al.* Targeting loss of the Hippo signaling pathway in NF2-deficient papillary kidney cancers. *Oncotarget* **9**, 10723–10733 (2018).
37. Chen, W. *et al.* Targeting renal cell carcinoma with a HIF-2 antagonist. *Nature* **539**, 112–117 (2016).
38. White, S. M. *et al.* YAP/TAZ Inhibition Induces Metabolic and Signaling Rewiring Resulting in Targetable Vulnerabilities in NF2-Deficient Tumor Cells. *Dev. Cell* **49**, 425-443.e9 (2019).
39. Marchand, A., Candi, A., Vanderhoydonck, B., Versele, M. & Gwaltney, S. WO2022072741: 1,2,3,4-tetrahydroquinoline derivates as inhibitors of the YAP/TAZ-TEAD activation for treating cancer. 338 (2022).
40. Imrichová, H., Hulselmans, G., Atak, Z. K., Potier, D. & Aerts, S. I-cisTarget 2015 update: Generalized cis-regulatory enrichment analysis in human, mouse and fly. *Nucleic Acids Res.* **43**, W57–W64 (2015).
41. Jing Yi1 *et al.* LATS1 and LATS2 regulate mouse liver progenitor cell proliferation and maturation through antagonism of the coactivators YAP and TAZ. *Hepatology* **64**, 1757–1772 (2016).
42. Jonkers, J. *et al.* Synergistic tumor suppressor activity of BRCA2 and p53 in a conditional mouse model for breast cancer. *Nat. Genet.* **29**, 418–425 (2001).
43. Jongsma, J. *et al.* A Conditional Mouse Model for Malignant Mesothelioma. *Cancer Cell* **13**, 261–271 (2008).
44. Pobbati, A. V *et al.* Targeting the Central Pocket in Human Transcription Factor TEAD as a Potential Cancer Therapeutic Strategy In Brief Accession Numbers 5DQ8 5DQE Article Targeting the Central Pocket in Human Transcription Factor TEAD as a Potential Cancer Therapeutic Strat. *Struct. Des.* **23**, 2076–2086 (2015).
45. Dupont, S. *et al.* Role of YAP/TAZ in mechanotransduction. *Nature* **474**, 179–184 (2011).
46. Ordóñez, N. G. The immunohistochemical diagnosis of mesothelioma: A comparative study of epithelioid mesothelioma and lung adenocarcinoma. *Am. J. Surg. Pathol.* **27**, 1031–1051 (2003).

47. Woyach, J. A. *et al.* Resistance Mechanisms for the Bruton's Tyrosine Kinase Inhibitor Ibrutinib. *N. Engl. J. Med.* **370**, 2286–2294 (2014).
48. Cunningham, R. *et al.* YAP/TAZ activation predicts clinical outcomes in mesothelioma and is conserved in in vitro model of driver mutations. *Clin. Transl. Med.* **13**, (2023).

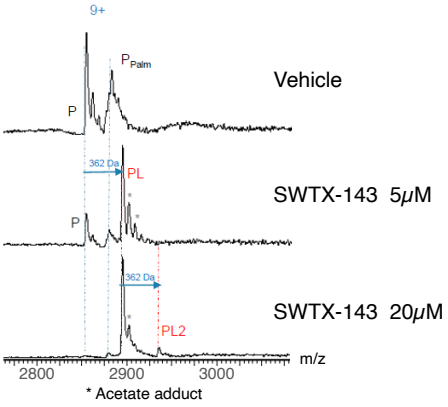
A SWTX-143



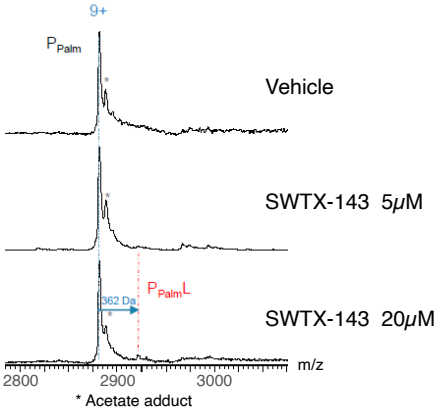
$C_{19}H_{18}F_3N_3O$

MW: 361,36 g/mol

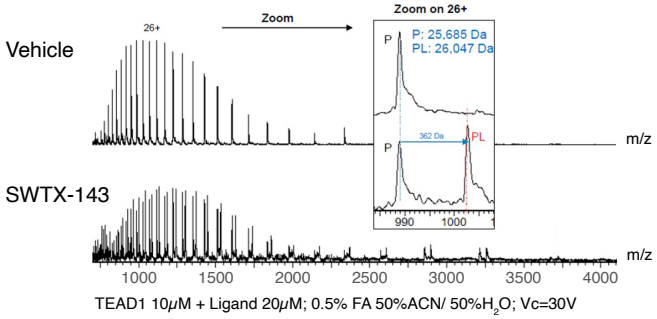
B Native TEAD1$^{R209-D426}$



C Fully palmitoylated TEAD1$^{R209-D426}$

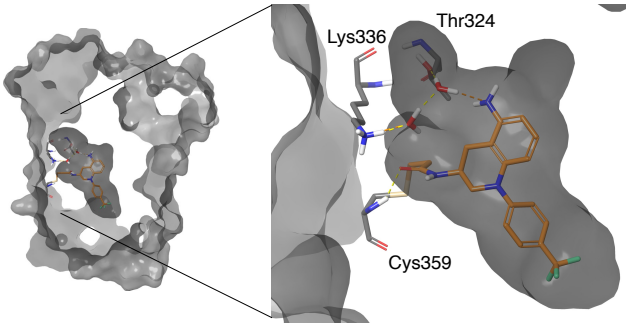


D Denaturating conditions - Native TEAD1$^{R209-D426}$



TEAD1 10µM + Ligand 20µM; 0.5% FA 50%ACN/ 50%H_2O; Vc=30V

E X-ray resolution of TEAD1/SWTX-143 co-crystal

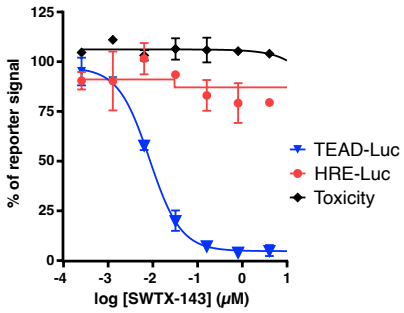


F Thermal Shift Assay Results

	TEAD1 (ΔTm-°C)	TEAD2 (ΔTm-°C)	TEAD3 (ΔTm-°C)	TEAD4 (ΔTm-°C)
SWTX-143-racemic	6.07	4.35	2.70	8.93
SWTX-143-A	6.22	5.74	-0.61	4.03
SWTX-143-B	6.95	5.00	3.78	8.92

Figure 1

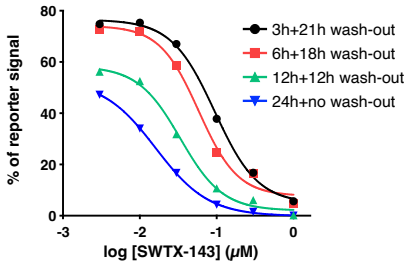
A TEAD Reporter Gene Assay



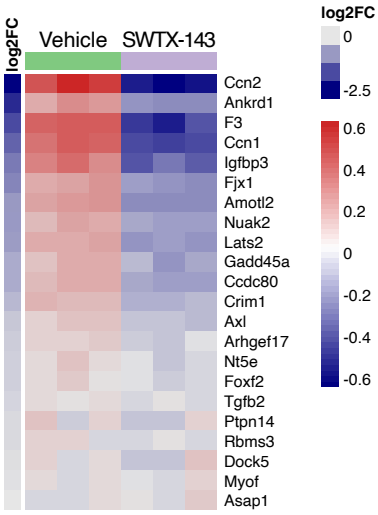
B

	TEAD RGA IC_{50} (μM)	HRE RGA IC_{50} (μM)	Toxicity IC_{50} (μM)
SWTX-143	0.012	>3	>3
SWTX-143-A	0.014	>3	>3
SWTX-143-B	0.009	>3	>3

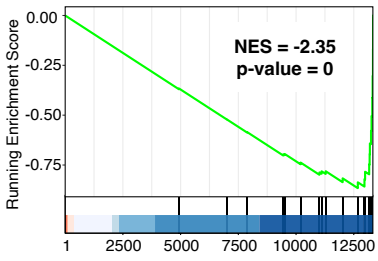
C SWTX-143 RGA wash-out



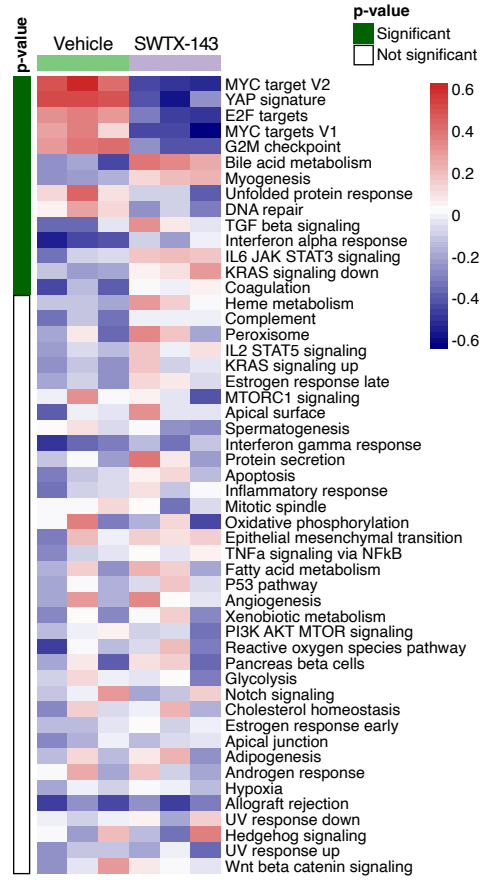
D YAP signature



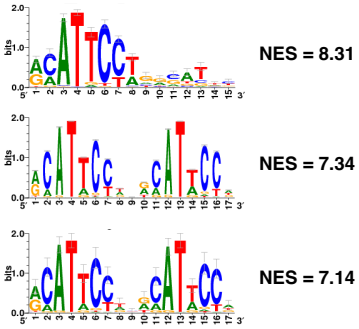
E Enrichment plot: YAP signature



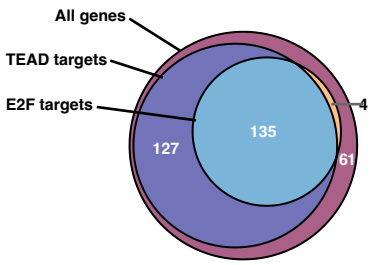
F Effects on signaling pathways



G Top 3 binding motives (all TEAD)



H Downregulated genes after SWTX-143 treatment



I Downregulated after SWTX-143 treatment

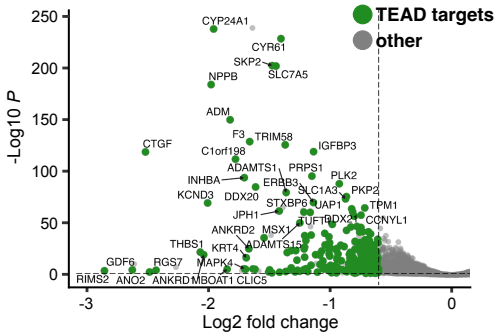
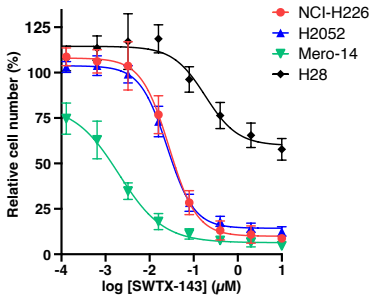


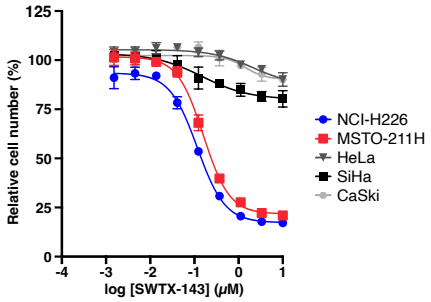
Figure 2

A Mesothelioma cell lines after 6 days of treatment



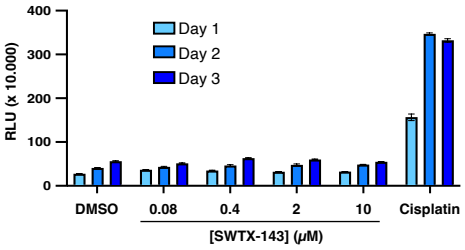
Cell line	Mutational status	IC_{50} (μM)
NCI-H226	$NF2^{LOF}$	0.033
NCI-H2052	$NF2^{LOF}$	0.019
Mero-14	$NF2^{LOF}$	0.005
H28	$NF2^{WT}$,$LATS^{WT}$	>10
NCI-H2452*	$NF2^{WT}$,$LATS^{WT}$	>10

B Mesothelioma and other cell lines after 6 days of treatment

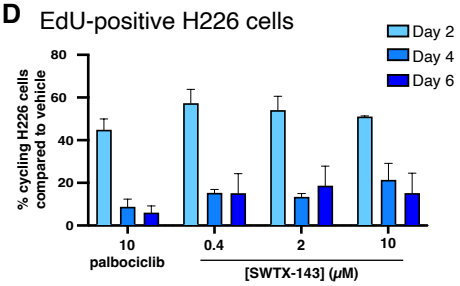


Cell line	Mutational status	IC_{50} (μM)
NCI-H226	$NF2^{LOF}$	0.122
MSTO-211H	$LATS1/2^{LOF}$	0.207
HeLa	$NF2^{WT}$,$LATS^{WT}$	>10
SiHa	$NF2^{WT}$,$LATS^{WT}$	>10
CaSki	$NF2^{WT}$,$LATS^{WT}$	>10

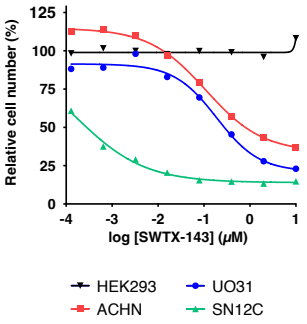
C Caspase3/7 activity assay



D EdU-positive H226 cells



E Kidney cell lines (6d treatment)



F Activity of SWTX-143 enantiomers

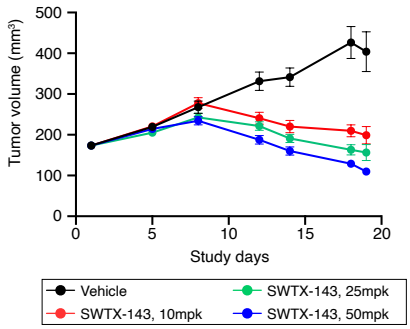
IC_{50} (μM)	SWTX-143	SWTX-143 A	SWTX-143 B
ACHN ($NF2^{mut}$/ $LATS2^{LOF}$)	0.110	0.315	0.038
SN12C ($NF2^{LOF}$)	0.0002	0.00014	0.0003
UO31 ($LATS2^{mut}$)	0.189	0.136	0.056
HEK293 ($NF2^{WT}$ /$LATS^{WT}$)	>10	>10	>10

G Comparison of different TEAD inhibitors

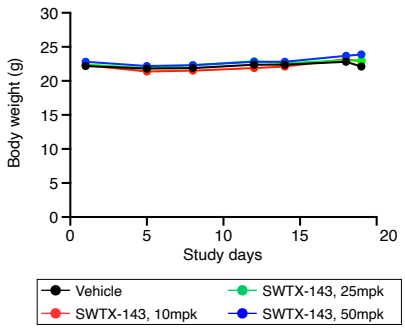
IC_{50} (μM)	**SWTX-143**	**K-975**	**VT104**
Reporter Gene Assay (HEK293)			
TEAD-Luc	0.012	0.008	0.015
HRE-Luc	>20	9.734	>20
Toxicity	>20	>20	>20
Cell proliferation			
H226	0.033	0.105	0.075
H2052	0.019	0.512	0.083
Mero-14	0.005	0.016	0.006
H28	>10	3.982	>10

Figure 3

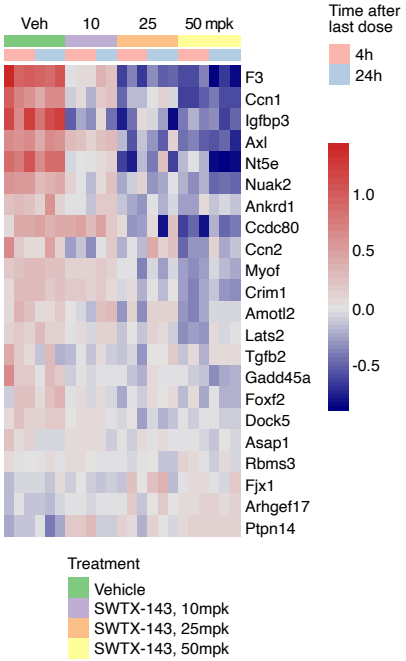
A Mean Tumor Volume



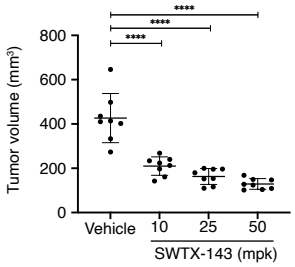
C Mean Body Weight



D YAP signature



B Tumor Volume at day 18



E Plasma exposure after 4h and 24h

SWTX-143 plasma PK in μM (total)	Sampling time	Day 18
10 mpk	4h	0.75
	24h	BLQ
25 mpk	4h	2.9
	24h	BLQ
50 mpk	4h	5.7
	24h	0.0057

Figure 4

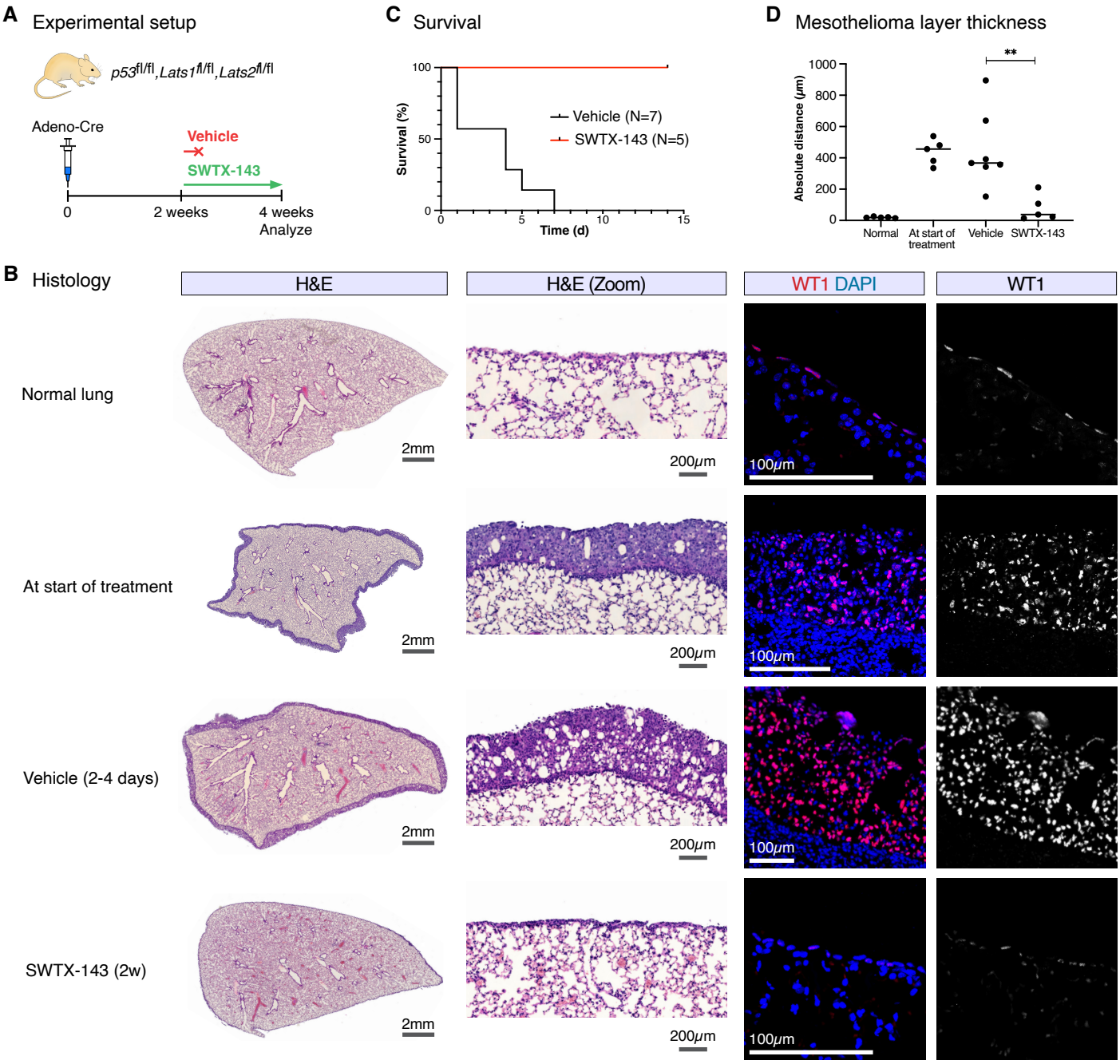
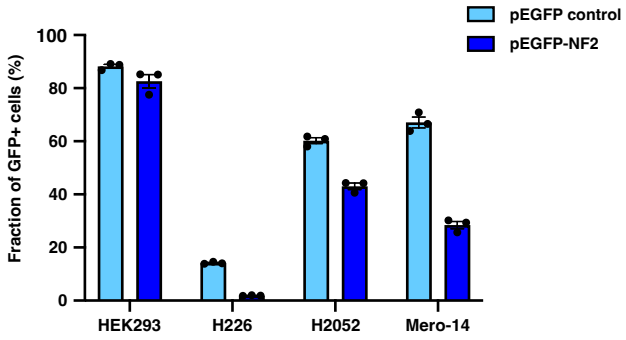

A
Experimental setup
p53fl/fl,Lats1fl/fl,Lats2fl/fl
Adeno-Cre
Vehicle
SWTX-143
0
2 weeks
4 weeks
Analyze
C
Survival
Survival (%)
Time (d)
Vehicle (N=7)
SWTX-143 (N=5)
D
Mesothelioma layer thickness
Absolute distance (μm)
**
Normal
At start of treatment
Vehicle
SWTX-143
B
Histology
H&E
H&E (Zoom)
WT1 DAPI
WT1
Normal lung
At start of treatment
Vehicle (2-4 days)
SWTX-143 (2w)
2mm
200μm
100μm

Figure 5

A Overexpression of NF2



B H2452 mesothelioma cells after 6 days of treatment

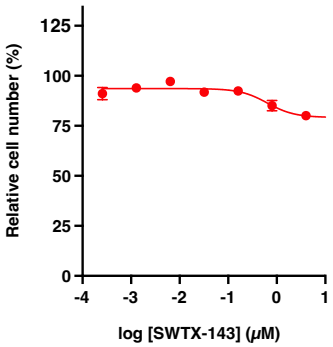
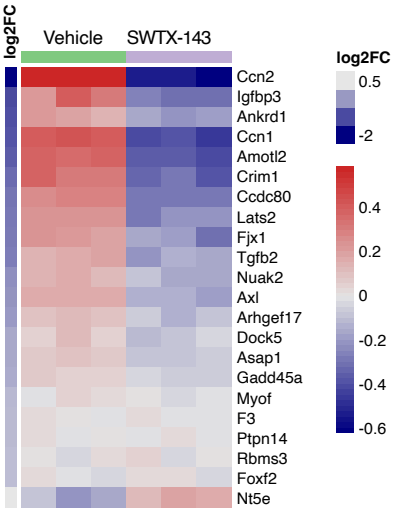


Figure S1

A YAP signature



B Enrichment plot: YAP signature

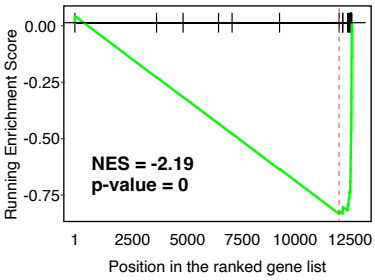


Figure S2

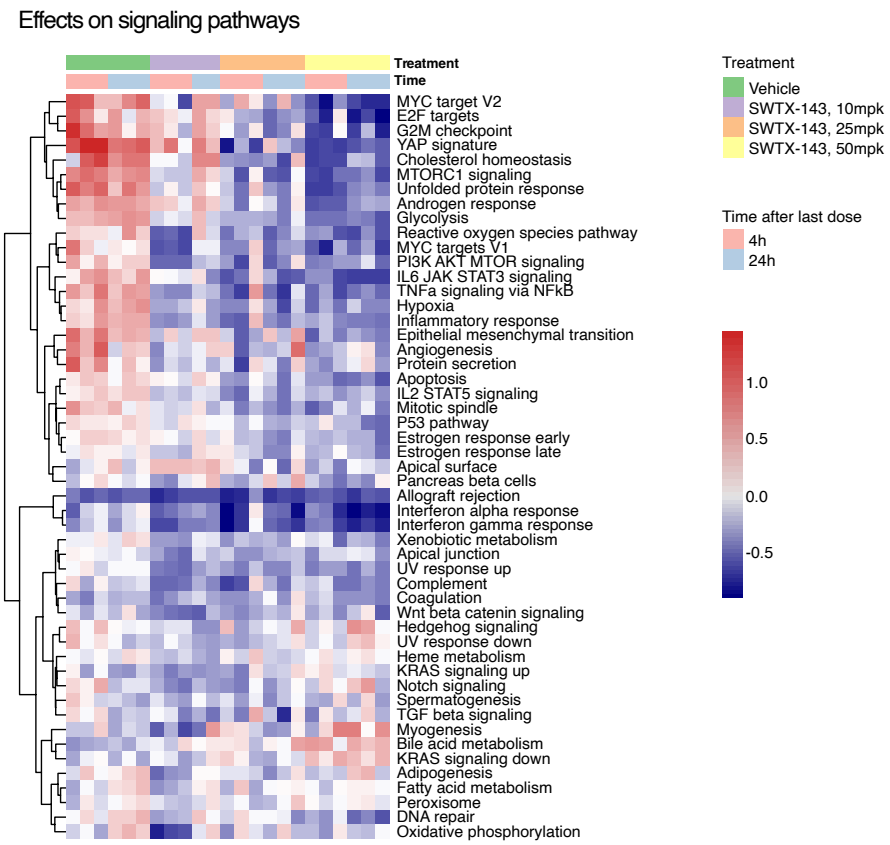
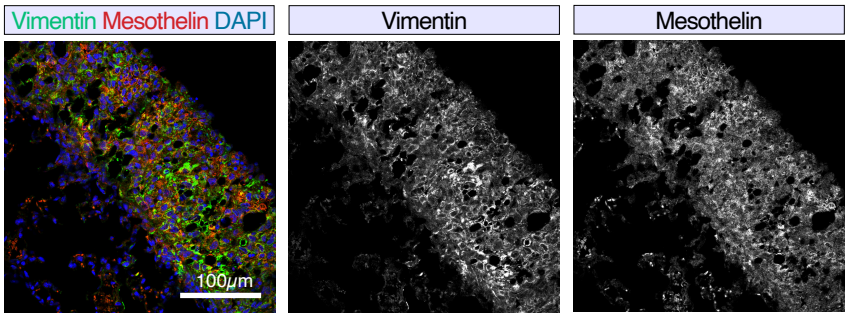

Effects on signaling pathways
Treatment
Time
MYC target V2
E2F targets
G2M checkpoint
YAP signature
Cholesterol homeostasis
MTORC1 signaling
Unfolded protein response
Androgen response
Glycolysis
Reactive oxygen species pathway
MYC targets V1
PI3K AKT MTOR signaling
IL6 JAK STAT3 signaling
TNFa signaling via NFkB
Hypoxia
Inflammatory response
Epithelial mesenchymal transition
Angiogenesis
Protein secretion
Apoptosis
IL2 STAT5 signaling
Mitotic spindle
P53 pathway
Estrogen response early
Estrogen response late
Apical surface
Pancreas beta cells
Allograft rejection
Interferon alpha response
Interferon gamma response
Xenobiotic metabolism
Apical junction
UV response up
Complement
Coagulation
Wnt beta catenin signaling
Hedgehog signaling
UV response down
Heme metabolism
KRAS signaling up
Notch signaling
Spermatogenesis
TGF beta signaling
Myogenesis
Bile acid metabolism
KRAS signaling down
Adipogenesis
Fatty acid metabolism
Peroxisome
DNA repair
Oxidative phosphorylation
Treatment
Vehicle
SWTX-143, 10mpk
SWTX-143, 25mpk
SWTX-143, 50mpk
Time after last dose
4h
24h
1.0
0.5
0.0
-0.5

Figure S3

A Mesothelioma marker staining



B Mesothelioma after 1 week of SWTX-143 treatment

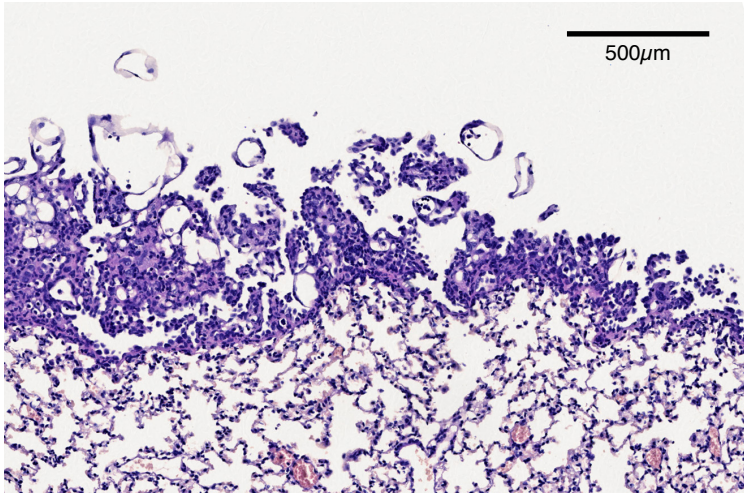


Figure S4